Mater Struct (2024) 57:19
https://doi.org/10.1617/s11527-023-02289-4

ORIGINAL ARTICLE

Effect of sulfidic mine tailings used as mineral admixtures on the hydration of common and alternative cements

N. P. Martins · J. Helser · M. Plötze · R. Snellings · G. Habert

Received: 18 August 2023 / Accepted: 17 December 2023 / Published online: 20 January 2024

Abstract In this work, we investigate the use of pyrite-rich tailings from an operational mine as mineral admixture in different cement matrices [Portland cement, calcium aluminate cement (CAC), and calcium sulfoaluminate cement (CSA)]. Hydration and microstructure changes were studied on cement pastes produced with a 30 wt% replacement of cement with tailings, up to 200 days. Based on our results, the effect of the tailings on the hydration of Portland cement is limited to a physical effect, and no sulfide-induced degradation is observed. In the CAC and CSA pastes, minor mineral phases present in the tailings chemically react, leading to changes in the mineral phase composition of CAC and CSA hydrated pastes. In addition, in all cement pastes studied, and more effectively in the CSA pastes, most of the metal(loid)s contained in the tailings were safely immobilized. Cement chemistry notation: C: CaO; A: Al_2O_3; F: Fe_2O_3; S: SiO_2; $\bar{S}$: SO_3; c: CO_2; H: H_2O.

Keywords Mine tailings · Hydration studies · Supplementary cementitious materials (SCMs) · Partial replacement

Supplementary Information The online version contains supplementary material available at https://doi.org/10.1617/s11527-023-02289-4.

N. P. Martins · G. Habert
Institute of Construction and Infrastructure Management, ETH Zürich, Stefano-Franscini-Platz 5, 8093 Zurich, Switzerland

N. P. Martins (✉) · R. Snellings
Sustainable Materials, VITO, Boeretang 200, 2400 Mol, Belgium
e-mail: natalia.piresmartins@vito.be

J. Helser · R. Snellings
Department of Earth and Environmental Sciences, KU Leuven, Celestijnenlaan 200E, 3001 Leuven, Belgium

J. Helser
Research Centre for Economics and Corporate Sustainability, KU Leuven, Warmoesberg 26, 1000 Brussels, Belgium

M. Plötze
Institute for Geotechnical Engineering, ETH-Zürich, Laura-Hezner-Weg 7, 8093 Zurich, Switzerland

1 Introduction

Mine tailings are the residual mineral waste generated during recovery of valuable metal-rich concentrate from the extracted ore. Estimations are that the global mine tailings generation is 7 billion tonnes each year [1]. Considering the gradual decreasing trend in ore grade in metallic mining [2, 3] and the growing demand for metals needed for the energy transition to a low-carbon economy [4], the overall volume of tailings is expected to increase strongly in the coming years and decades [5].

Currently, the large majority of tailings are deposited and contained in storage facilities [6]. Sulfidic tailings, i.e. tailings that contain sulfide minerals,

with pyrite (FeS_2) being the most common one, require specific containments to avoid contamination of the environment. When exposed to the atmosphere, sulfide minerals tend to oxidize and produce highly acidic water rich in sulfate and metal(loid)s. This phenomena is known as acid mine drainage (AMD) and is the largest environmental problem faced by the mining industry today [7].

To close material loops in the circular economy model, technologies to efficiently extract valuable metals from tailings and to safely use or store the remaining metal-depleted mineral matrices must be developed [8]. In terms of potential demand, significant opportunities for the use of tailings exist as raw materials for use in the construction sector. Potential high-volume applications are their use in large civil engineering works such as embankments, fills or road base, as alternative aggregates, or as raw materials for cement-bound applications, where they can potentially substitute part of the fines and the cement as filler, or as reactive material contributing to the cement performance [9].

Only few publications have addressed the use of mine tailings as a partial replacement for cement, with the particular case of sulfidic tailings having received even less attention [10]. This is partially explained by incompliance of sulfidic tailings to industry standards, especially in terms of their chemical composition i.e., sulfur contents above the allowed limits in common standards for cements i.e., 3–5 wt% [11–13], and high concentrations of residual metal(loid)s [10] i.e., as high as 9300 ppm in terms of individual metal(loid) concentration, as Pb in [14].

When sulfidic minerals such as pyrite, pyrrhotite, and marcasite are present in concrete aggregates, their oxidation in the presence of water is known to lead to several reactions that can cause concrete degradation. This is mainly due to the formation of reaction products such as iron hydroxides and sulfate-containing phases (e.g., gypsum, ettringite, thaumasite) [15, 16]. Primary expansion results from the formation of iron hydroxides, since the products have a higher volume than the initial reactants. Secondary expansion, referred to in the literature as internal sulfate attack (ISA), arises from the reactions between the released sulfate and cement hydrates long after the concrete has hardened [16, 17]. The reaction with Ca^{2+} from certain hydration products ($Ca(OH)_2$ and C–S–H gel) can produce gypsum, while additional Al-bearing phases, i.e., monosulfate, are needed to form ettringite and thaumasite. The decalcification of C–S–H is extremely undesirable as it results in the weakening of the paste. The tight containment of these products in the aggregates can lead to expansion and cracking or even premature failure of the concrete.

In sulfidic tailings, the reactive sulfide minerals are typically present in smaller particle size, which could enhance their reactivity. On the other hand, their distribution in the more porous binder phase may avoid the generation of expansion pressure. Instead, if reactive sulfidic tailings are used as mineral admixtures in cement, they could potentially contribute to the cement performance by supplying additional hydration products. Moreover, the mobility and availability of potentially hazardous elements could be reduced by incorporation into the cement hydration products. This work investigates the possibility of incorporation of sulfidic mine tailings as a partial replacement for cement in different types of cements with contrasting cement chemistries and hydration mechanisms. The focus of this work is on the identification of the effects of the tailings on the hydration of Portland cement (PC), calcium aluminate cement (CAC), and calcium sulfoaluminate cement (CSA), and assessing the environmental compatibility of the replacement strategy by means of leaching tests.

2 Materials and methods

2.1 Materials

Sulfidic tailings were used as admixtures in cement-tailings pastes containing 70 wt% cement and 30 wt% tailings. The replacement ratio was fixed at a moderate level—equivalent to CEM II/B—because it could potentially result in noticeable environmental gain in terms of reduction of CO_2 emissions per kg of blended cement and would represent a potentially high-volume valorization route for the residue. A higher replacement ratio was not adopted because it would be significantly above the current typical European average. The tailings originated from the operational underground Cu–Zn mine of Neves-Corvo, in Portugal, located within the western part of the Iberian Pyrite Belt [18]. The original fresh thickened tailings consisted of a

wet sludge when received. In this study, the tailings were used in the form of a fine powder obtained after homogenization and drying of the sludge at 40 °C in a vacuum oven for approximately a week. The dried material was then homogenized, sampled, and vacuum packed to prevent changes in mineralogy by oxidation of the sulfides. Quartz powder was used as an inert filler at the same replacement ratio in the reference pastes. Care was taken to use a material with similar particle size distribution as the tailings in order to account for the filler effect, as it was done in another study [19].

To study the chemical interactions between the tailings and the different cements, cement-tailings pastes were produced using three cement types. Commercial Portland Cement (CEM I 42.5N) (PC) and Calcium Aluminate Cement (Cement Fondu) (CAC), and a synthetic Calcium SulfoAluminate clinker (CSA) were used in this study. The CSA clinker used was produced at a laboratory furnace (LHT 16/R, Nabertherm) using reagent grade Al_2O_3, $CaSO_4{\cdot}2H_2O$, and $CaCO_3$ (readers are referred to Online Appendix A, Figure A-1, for more details).

The particle size distribution (PSD) of the materials was measured in isopropanol suspensions using a Horiba LA350 particle size analyser. The results for the different cement types, tailings, and quartz are presented in Online Appendix A (Figure A-2). The specific surface area was measured using BET analysis of N_2 sorption data and their density was determined by He-pycnometry. The chemical composition of the materials was measured by X-ray fluorescence (XRF) spectroscopy. The mineralogical composition was investigated by X-ray diffraction (XRD). The results of chemical, physical, and mineralogical analyses of the starting materials are summarized in Table 1.

Both the tailings and the quartz powder used in this study have 67 wt% of the particles below 12 µm. The differences, however, are in the coarser fraction of both admixtures and on the specific surface area of the powders. While the tailings contain particles up to 300 µm, the coarser fraction of quartz ranges only up to 50 µm.

The synthetic CSA is finer than the commercial cements (PC and CAC). PC has a typical mineral phase composition, containing C_3S, C_2S, C_4AF, C_3A, and calcite as major phases. The major phases present in CAC are CA, C_4AF, C_2S, and C_3A, in addition to minor amounts of $C_{12}A_7$. The CSA used consists mostly of $C_4A_3\bar{S}$ and anhydrite ($CaSO_4$).

According to the chemical analysis, the tailings contain potentially toxic metal(loid) such as Zn, Cu, As, and Pb. If such metal(loid)s are mobile in sufficiently high concentrations, the tailings can be considered to pose environmental and health risks. The high sulfur content is present mostly in sulfidic form. The sulfidic minerals present in the tailings are pyrite (46.4 wt%) and chalcopyrite (0.5 wt%), in addition to quartz, phyllosilicates (muscovite, biotite, chlorite), and other minor minerals (carbonates, gypsum). The sulfidic tailings present 24.9 wt% of mass loss when heated from 30 to 950 °C under N_2. As indicated in the curves obtained by thermogravimetric analysis (TGA-MS) (Online Appendix A, Figure A-3), the main weight losses are due to the desulfurization of sulfidic minerals, the dehydroxylation of micas, and decarbonation, which typically takes place above 400 °C in carbonate minerals (siderite, dolomite). The weight loss between 100 and 200 °C corresponds to dehydration of gypsum. No CO_2 release is observed up to 400 °C, which indicates the absence of organic matter. The TG-MS analysis of a sample of similar composition of the Neves Corvo fresh tailings was analyzed under air atmosphere and reported by [20].

2.2 Paste preparation

The hydration kinetics of the cements blended with sulfidic tailings was followed on cement pastes by measuring the heat of hydration using isothermal calorimetry. The evolution of phase composition was studied using XRD and TGA. The pore structure of the hydrated pastes was analyzed by mercury intrusion porosimetry (MIP). Scanning electron microscopy (SEM) was used to have an overall impression of the microstructure of the hydrated materials. The environmental compatibility of the cements was evaluated based on leaching tests on cement pastes.

Dry blends of 70 wt% cement and 30 wt% tailings—or quartz, in the reference—were used to produce the pastes. Cement pastes of PC and CAC were prepared at the water to cement (w/c) mass ratio of 0.57 (equivalent to a water to total solids ratio (w/s) of 0.4, when accounting also for the tailings/quartz). A $w/c = 0.86$ (equivalent to $w/s = 0.6$) was used in the CSA pastes because this cement type has a higher

Table 1 Physical properties, chemical, and mineralogical composition of the input materials used in this study

	PC	CAC	CSA	Tailings	Quartz
Oxide composition (%)					
Na_2O	< 0.7	1.8	1.6	3.1	
MgO	2.2	1.3	0.7	1.3	
Al_2O_3	5.8	45.2	53.4	8.7	
SiO_2	20.8	4.3		24.0	99.8
P_2O_5	0.7	0.5			
SO_3	2.4	0.1	14.0	33.8	
K_2O	0.8			0.4	
CaO	59.9	30.7	29.7	0.8	
TiO_2	0.2	1.1		0.1	0.02
MnO		0.1			
Fe_2O_3	2.2	12.0		24.2	
V (mg/kg)				43	
Cr (mg/kg)				56	
Cu (mg/kg)				2940	
Zn (mg/kg)				6300	
As (mg/kg)				3670	
Sn (mg/kg)				595	
Sb (mg/kg)				218	
Pb (mg/kg)				2440	
Mineralogy (wt%)					
C_3S	66.5 (0.9)				
C_2S	10.6 (0.7)	7.7 (0.7)			
C_4AF	8.2 (0.5)	20.0 (0.8)			
C_3A	3.7 (0.5)	7.1 (0.6)			
CA		61.6 (0.7)			
$C_{12}A_7$		3.7 (0.3)			
$C_4A_3\bar{S}$			92.4 (0.5)		
Lime			0.7 (0.1)		
Periclase	1.4 (0.1)				
Anhydrite			6.9 (0.5)		
Gypsum	2.1 (0.3)			1.9 (0.1)	
Syngenite	2.3 (0.6)				
Calcite	4.5 (0.9)				
Dolomite				1.9 (0.1)	
Siderite				2.5 (0.1)	
Quartz	0.7 (0.1)			24.9 (0.2)	99.5 (0.2)
Cristobalite				0.5 (0.2)	
Pyrite				46.4 (0.2)	
Chalcopyrite			0.5 (0.1)		
Muscovite			4.7 (0.1)		
Biotite				3.5 (0.1)	
Chlorite				13.7 (0.2)	
SSA (m^2/g)	0.88	0.77	0.97	0.95	1.73
Density (g/cm^3)	3.11	3.23	2.65	3.6	2.64
d_{10} (µm)	1.6	1.4	1.6	3.2	3.0
d_{50} (µm)	14.0	13.1	6.8	8.3	9.6

Table 1 (continued)

	PC	CAC	CSA	Tailings	Quartz
d_{90} (μm)	43.6	48.2	13.4	53.5	19.1

The estimated standard deviations from the XRD-Rietveld analysis of each sample are given in parenthesis

water demand [21] and an appropriate fluid consistency was desired. To minimize bleeding in the pastes, a small fraction of the mineral admixture (quartz or tailings) was replaced by bentonite (below 2 wt% of solids). After equilibrating the input materials at 20 °C, the solids were premixed by hand and subsequently mixed with ultrapure water using an overhead propeller mixer at 1600 rpm for 2 min. Immediately after mixing, 15 g of the pastes were placed into glass calorimeter flasks, sealed air-tight, and lowered into the measurement positions of the isothermal calorimeter. The remaining paste was cast into cylindrical HDPE containers and sealed air-tight using parafilm. The pastes were stored at 20 °C and sampled after 1, 7, 14, 28, 90, and 200 days of age. At each age, four disks of 2–3 mm thickness were cut from the hardened cylinders using a laboratory diamond saw. Two disks were crushed and hydration stopped by isopropanol solvent exchange following [22]. After hydration stoppage, the samples were stored in a desiccator under vacuum until they were measured by TGA and XRD. Two other disks were kept in isopropanol for 7 days (with three exchanges of isopropanol) and dried in a desiccator under vacuum prior to the preparation for MIP and SEM analyses. One whole cylinder of each mix was used in the leaching tests at 200 days, without undergoing hydration stoppage.

2.3 Isothermal calorimetry

Heat flow and cumulative heat results were obtained from isothermal calorimetry measurements using a TAM Air calorimeter that was pre-equilibrated and calibrated for measurement at 20 °C. The heat release of the pastes was measured for 28 days after mixing. The mixing was done outside the calorimeter, as described in the section “Paste preparation”. The minimum heat flow in the induction period was taken as initial time for the calculation of the cumulative heat.

2.4 Thermogravimetric analysis (TGA)

Thermal analysis was conducted for the characterization of the tailings and to assist the identification and quantification of hydration products in the hydrated cement pastes. Simultaneous TGA-MS was performed on a Netzsch STA 449C instrument connected to a quadrupole mass spectrometer (MS) 403 C Aëolos under N_2 atmosphere (50 mL/min flow rate), in the 25–1000 °C temperature range, using a heating rate of 10 K/min. Samples of approximately 50 mg were measured.

2.5 X-ray diffraction (XRD)

The mineralogy of the anhydrous materials and cement pastes hydrated until 28 days was measured on powdered specimens (< 63 μm) using a PANalytical Empyrean diffractometer in Bragg–Brentano geometry, with a Co-Kα X-ray source. The powder samples were step-scanned at room temperature from 5 to 120°2θ (step width 0.013°2θ, 0.15 s per step). A Bruker AXS D8 Advance Bragg–Brentano X-ray diffractometer with a Co-Kα X-ray source was used to measure the powders of samples hydrated for 90 and 200 days. The measurements were made at room temperature from 4 to 80°2θ (step width 0.02°2θ, 2 s per step). Qualitative phase analysis of the XRD data was carried out using the X’Pert Highscore Plus v 4.7a software package by PANalytical and quantitative analysis was done using the Rietveld method in the Profex software package [23]. The chemically bound water values obtained by TGA were used in the back-calculation of the phase composition of the hydrated pastes to a common basis. The rescaled results were then used to calculate the degree of hydration (DoH) of cement.

2.6 Mercury intrusion porosimetry (MIP)

A few grams of material were taken from the broken disks to study the pore structure of hydrated pastes by MIP. The measurement was performed using a combined instrument (Pascal 140 + 440, POROTEC) at a maximum pressure of 400 MPa. The pore size distribution in the macro- and mesopore range (pore radius 58,000-1.8 nm) was determined according to the Washburn equation [24], which gives a relationship between pressure and pore size, considering a surface tension of mercury equal to 0.48 N/m, and a wetting angle of 135°.

2.7 Scanning electron microscopy/energy dispersive x-ray spectroscopy (SEM/EDS)

A JEOL JSM 6400 scanning electron microscope operating in backscattering (BSE) mode was used at an accelerating voltage of 15 kV to observe the microstructure of the hydrated pastes. The polished sections studied by SEM were made by vacuum-embedding a piece of broken disk in cold epoxy resin and polishing it using diamond abrasives to produce a flat mirror surface, which was then carbon-coated. EDS was used in the production of elemental maps to assist the identification of features in the micrographs.

2.8 Thermodynamic modelling

Thermodynamic modelling of phase assemblage was performed for the CAC system to predict alterations in the hydrated phases due to the presence of carbonates in the tailings. For that, the Gibbs Energy Minimization Software (GEMS, version 3.5) [25–27] was used and the thermodynamic properties of components were taken from the PSI-Nagra and CEMDATA18 [28] databases.

2.9 Leaching tests

The European compliance one stage batch leaching test (EN 12457-2, 2002) was performed on samples that hydrated for 200 days. The samples were crushed to a particle size < 4 mm on the day of the experiment. Deionized water was added to the sample at a liquid to solid ratio of 10 l/kg in a centrifuge tube and shaken at 100 rpm on a reciprocal shaker for 24 h. After shaking, the tubes were centrifuged for 10 min at 3200 rpm. Then, the pH was measured and the supernatant was filtered using a syringe and a 0.45 µm Chromafil filter. The leachates were stored in the refrigerator (at 5–10 °C) for 2 days until analysis by induced coupled plasma-optical emission spectroscopy (ICP-OES Varian 730 ES).

3 Results and discussion

3.1 Effect of tailings on cement hydration kinetics

The impact of the tailings on the hydration kinetics of PC, CAC, and CSA is illustrated in Fig. 1. The tailings are observed to cause a later start of the acceleration period, as seen on the heat flow curves (left). The increased cumulative heat (right) observed with the replacement of cement with tailings was significant—over 5% 28 days after mixing—only for the CSA cement. The cumulative heat values of CSA − Q and CSA − T samples after 28 days are 425 and 451 J/g of CSA cement, respectively. For PC and CAC, the increase in cumulative heat released from the pastes containing tailings was only 0.7% and 0.4%, respectively, when compared to the quartz-containing pastes. The late onset of reaction observed for the CSA cement in the heat flow curves in Fig. 1 in both the reference and tailings-containing paste could be related to the higher $w/c = 0.86$ used for CSA, in contrast to the $w/c = 0.57$ used for both CAC and PC pastes (i.e., higher w/c might delay hydration kinetics) or, most likely, to the insufficiency of extra sulfate in CSA (see Figure A-4 in Online Appendix A).

The slight extension of the dormant period observed in the tailings-containing PC, CAC, and CSA pastes is suggested to be attributed to chemical interactions between the cement mineral phases and specific species contributed by the tailings that are known to delay cement hydration. The effect of metal(loid)s on cement hydration is not straightforward and has been subject of many studies, especially in PC, but also in CSA and CAC. It has been observed, for instance, that the hydration of PC was retarded in the presence of Zn [29], while a gypsum-free CSA is accelerated by Zn^{2+} cations [30], or that Cd has a clear retarding effect on the hydration of CSA [31]. Apparently conflicting data might be explained by the combined effect of several metal species acting on the hydration of the

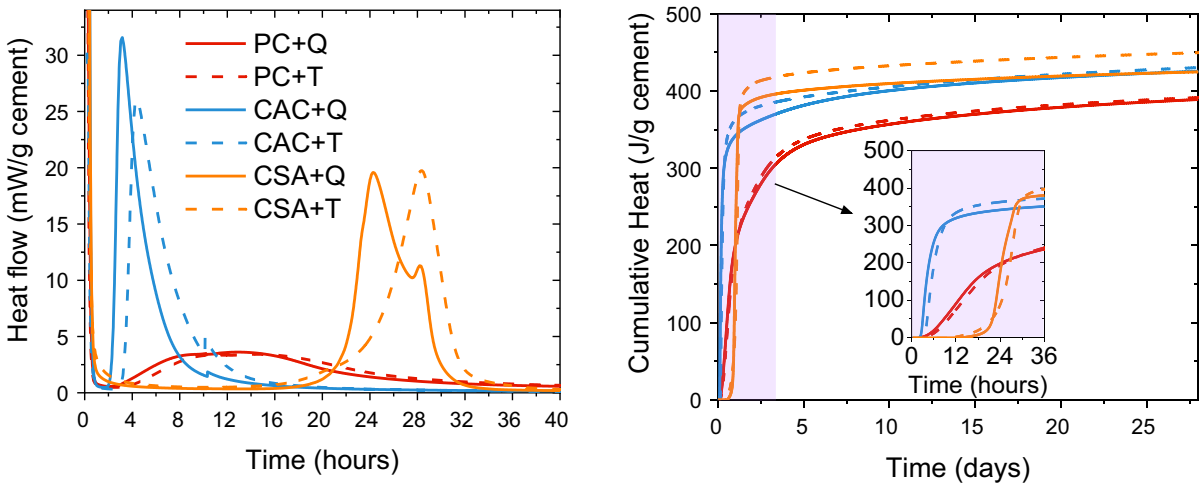

Fig. 1 Heat flow (left) and cumulative heat (right) curves of cement pastes produced using 30% replacement with quartz (Q) (reference, continuous lines) and tailings (T) (dashed lines) of PC (red), CAC (blue), and CSA (orange). (Color figure online)

clinker phases. In the case of CSA, the presence and content of gypsum can make the analysis even more complex [30, 32]. Figure A-5 (in Online Appendix A) shows that metal(loid)s such as Zn, Cd, Cu, and Pb are released from the tailings during single extractions at pH 11 and 13, suggesting their release during the early hydration of cement. Whereas it is uncertain whether at such concentrations those species could alter the kinetics of cement hydration at all, their presence in the leachates could be related to the slight retardation observed in the heat flow curves of the tailings-containing pastes.

In the CSA + T paste, the reaction started at a lower rate, as indicated by the initial slope of the main hydration peak, which results in the exothermic hydration peak taking place 28 h after mixing, 4 h later than the reference paste. Moreover, the shoulder on the right side of the main hydration peak was present only in the reference paste. That shoulder is frequently observed in calorimetric curves and corresponds most probably to sulfate depletion, being characterized by the formation of monosulfate. It is observed when the amount of calcium sulfate added to the clinker is insufficient to complete the hydration reaction of ye'elimite to ettringite [33]. In the tailings-CSA paste, the absence of the shoulder is most likely caused by the provision of additional sulfate by the tailings.

3.2 Hydration of Portland cement (PC)—tailings pastes

The XRD results of the PC pastes are presented in Fig. 2, which show that the presence of tailings only marginally affects the dissolution of the PC clinker phases—C_3S, C_2S, C_3A, C_4AF—and the formation of hydration products—ettringite ($C_6A\bar{S}_3H_{32}$), hemicarbonate ($C_4Ac_{0.5}H_{12}$), monocarbonate (C_4AcH_{11}) and portlandite (CH)—in agreement with the isothermal calorimetry curves. The stabilization of ettringite and monocarbonate in the long term is typically observed in PC pastes containing calcium carbonates [34]. Despite presenting the same hydrated phase assemblage, the PC + T paste presented a slightly higher content of ettringite and AFm as calculated by XRD-Rietveld, which was confirmed by TGA (Online Appendix A, Figure A-6). This is likely to have resulted from minor amounts of additional sulfate and aluminium contributed by the tailings. Despite the partial dissolution of phyllosilicate minerals present in the tailings—muscovite, biotite—in the longer term (200 days), the hydrated phase composition of the tailings-containing paste is equivalent to that of the reference paste at that age.

Additionally, MIP results (Fig. 3) show that a continuous reduction of the total pore volume and refinement of the pore structure, which are a result

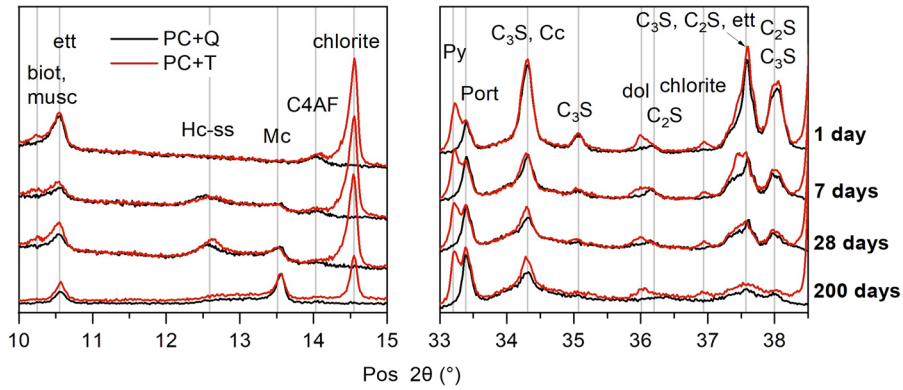

Fig. 2 XRD patterns of PC pastes containing tailings (red) and reference paste (black) hydrated for 1, 7, 28, and 200 days. Biot: biotite, musc: muscovite, dol: dolomite, ett: ettringite, Hc-ss: hemicarbonate solid solution, Mc: monocarbonate, Py: pyrite, Port: portlandite. Two parts of the patterns are shown to highlight the formation of hydration products (left) and dissolution of cement phases (right). The XRD patterns were normalized to the intensity of the main peak of quartz ($d = 3.34$ Å). (Color figure online)

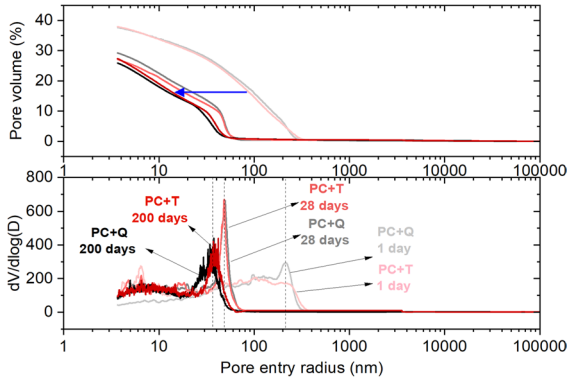

Fig. 3 Cumulative pore volume (top) and pore size distribution (bottom) of PC pastes containing tailings (shades of red) and reference pastes (shades of grey) hydrated for 1, 28, and 200 days. The blue arrow is a guide to the eyes and represents the order of the pore volume cumulative curves, according to the increasing age of the hydrated pastes. (Color figure online)

of the increasing formation of hydration products, are observed for both PC + Q and PC + T pastes. The pore structure of the PC + T hydrated paste is preserved during the entire period of analysis. Based on the MIP results and on the known link between the evolution of the pore size distribution and the strength development of cementitious systems, we could expect that the strength of the mixes is not negatively affected by the tailings within the first 200 days of age. Although expected, those results must be confirmed in future studies. Overall, the impact of the sulfidic tailings on the hydration of Portland cement was found to be small and limited to a slight retardation and increase in the ettringite content of the pastes.

3.3 Hydration of calcium aluminate cement (CAC)—tailings pastes

The XRD patterns of the CAC pastes are shown in Fig. 4. They show that the decrease in peak intensities of the CAC clinker phases—CA, C_2S, C_3A and C_4AF—took place similarly for both tailings-containing and reference pastes. This points out to a similar rate of reaction of the clinker phases. Both pastes presented the same hydrated phase assemblage (AH_3, CAH_{10}, C_2AH_x, and C_3AH_6), which is in agreement with CA pastes hydrated at 20 °C [35], but the relative amounts of the calcium aluminate hydrates evolved with the hydration age. The phase C_2AH_x refers to C_2AH_8 and two other hydrates with similar layer distance and water contents of 8.2 and 7.5 molecules H_2O per structure formula unit, which have d_{001} equal to 10.75 Å, 10.88 Å, and 10.45 Å, respectively [36]. In the XRD patterns (Fig. 4), the corresponding 2θ range is indicated as C_2AH_x.

In CAC where $CaO/Al_2O_3 \approx 0.9$ at temperatures above 19 °C (this study), the main clinker phase, CA, hydrates to form CAH_{10}, C_2AH_8, and AH_3, according to the following hydration reactions [37]:

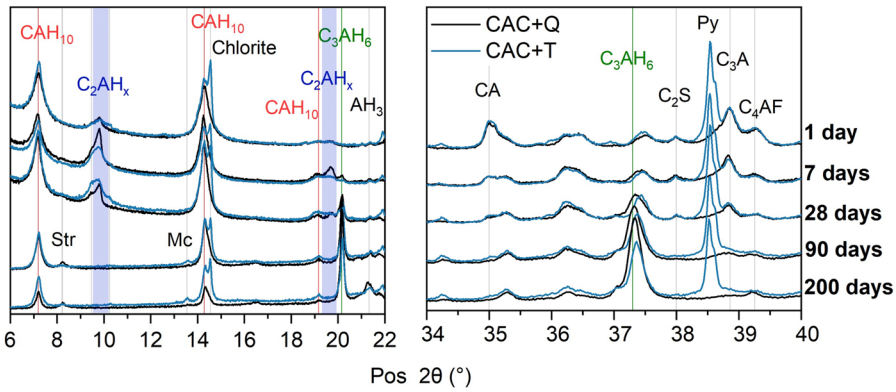

Fig. 4 XRD patterns of CAC pastes containing tailings (blue) and reference paste (black) hydrated for 1, 7, 28, 90, and 200 days. Str: strätlingite, Mc: monocarbonate, Py: pyrite. The peaks of the different calcium aluminate hydrates are indicated by reference lines: red (CAH_{10}), blue (C_2AH_x), and green (C_3AH_6). The XRD patterns were normalized to the intensity of the main peak of quartz (d = 3.34 Å). (Color figure online)

$$CA + 10\,H \rightarrow CAH_{10} \quad (1)$$

$$2\,CA + 11\,H \rightarrow C_2AH_8 + AH_3 \quad (2)$$

The calcium aluminate hydrates CAH_{10} and C_2AH_8 are thermodynamically less stable than C_3AH_6 and AH_3 [35], therefore conversion reactions are expected to take place over time:

$$3\,C_2AH_8 \rightarrow 2\,C_3AH_6 + AH_3 + 9\,H \quad (3)$$

$$3\,CAH_{10} \rightarrow C_3AH_6 + 2\,AH_3 + 18\,H \quad (4)$$

In this study, while CAH_{10} persisted up to 200 days, the intensities of peaks corresponding to C_2AH_x phases decreased with time and they finally vanished by 90 days, as more C_3AH_6 and AH_3 formed. After 90 days, CAH_{10} was also seen to decrease, particularly in the CAC + Q paste. The extent of the conversion reactions—or degree of conversion (DoC)—can be calculated at different ages, as proposed in [38] (Eq. 5), using quantitative data obtained from XRD. Due to a lack of structure file for phases C_2AH_x, those phases were not included in the calculation.

$$DoC = \frac{C_3AH_6}{C_3AH_6 + CAH_{10}} \quad (5)$$

As it can be seen in Fig. 5, the conversion reactions take place at a higher rate in the reference

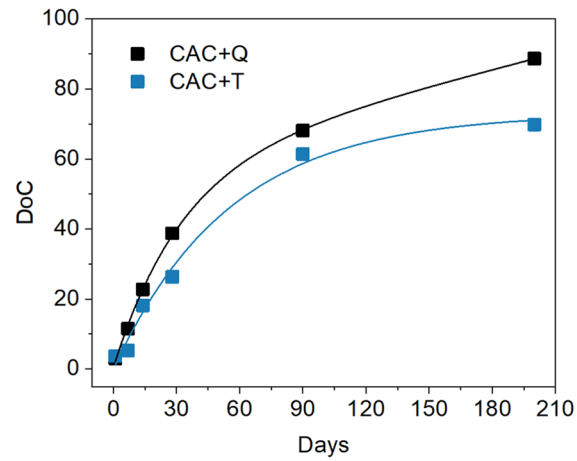

Fig. 5 Degree of conversion (DoC) of CAC pastes calculated based on quantitative XRD results

paste. At 200 days, the DoC of the reference paste is nearly 90%, against 70% in the tailings-containing paste. Therefore, it may be inferred that the presence of tailings helps to stabilize and preserve the CAH_{10} phase, and consequently suppress the formation of C_3AH_6 and reduce the DoC. It is known that substitution of certain anions in the C_2AH_8 interlayers increase the stability of the structure and reduces the rate at which conversion to C_3AH_6 occurs [39]. For that reason, anions such as CrO_4^{2-}, NO^{2-}, SO_3^{2-}, and MnO^{4-} serve as stabilizers for CAC [40]. The results in this study suggest that,

in the presence of sulfidic tailings, the stabilizing effect could be extended to the CAH_{10} phase.

After 90 days, different newly formed products are observed in the pastes. The formation of modest amounts (< 8%) of monocarbonate (C_4AcH_{11}, indicated as Mc in Fig. 4) was observed by XRD after 90 days only in the tailings-containing hydrated paste. Although monocarbonate may form as a transient product of carbonation in hydrated CAC systems [37], it is more likely that it results from the reaction between converted products and carbonates present in the tailings. This mechanism has been previously observed in mixtures of CAC and calcite [41–43]. In the CAC + T paste, the formation of C_4AcH_{11} possibly results from the slow dissolution of siderite and/or dolomite present in the tailings, and could also partially justify the reduced amount of C_3AH_6 observed experimentally by XRD and TGA. This hypothesis was further explored by thermodynamic modelling using GEMS in a simplified CA + dolomite ($CaMg(CO_3)_2$) + siderite ($FeCO_3$) system at 20 °C. The proportions of CA, siderite, and dolomite in the input were kept the same as in the anhydrous CAC + T paste (97.1 g of CA, 1.69 g of siderite, and 1.28 g of dolomite). The results are given in Fig. 6 in volume (cm^3/100 g of solids) for three different w/s ratios, as a function of the extent of dissolution of the siderite and dolomite, which was varied from 0 to 100%.

According to the modelling results shown in Fig. 6, the formation of carbonate-containing AFm phases is predicted in the system at the expense of C_3AH_6, but the composition of the AFm phase formed is dependent on the availability of water and on the extent of dissolution of the carbonates. For $w/s = 0.40$ (Fig. 6a), when excess water is not available, monocarbonate (C_4AcH_{11}) is predicted to form and its content increases with the increase in the extent of dissolution of the carbonates. In the presence of excess water ($w/s = 0.55$, Fig. 6c), hemicarbonate ($C_4Ac_{0.5}H_{12}$) is predicted to form and the content of this phase is only limited by the availability of dissolved carbonate. That leads to a significant decrease in the content of C_3AH_6 and an increase in the total volume of solids, which can bring potential benefits in terms of space filling. When $w/s = 0.45$ (Fig. 6b), both carbonate-AFm compositions are predicted: $C_4Ac_{0.5}H_{12}$ is the dominant one when the extent of dissolution of carbonates is below 20%; and C_4AcH_{11} is dominant above that and in the absence of surplus water (similar to Fig. 6a). It must be noted that the actual formation of carbonate-AFm hydrates in the cement paste highly depends on the kinetics of the reaction between the carbonate minerals and CAC hydrates, which was not taken into account in the simplified thermodynamic calculations. Therefore, differences may exist between the products predicted in the model and the products actually formed in the system. Nevertheless, Fig. 6 shows that the formation

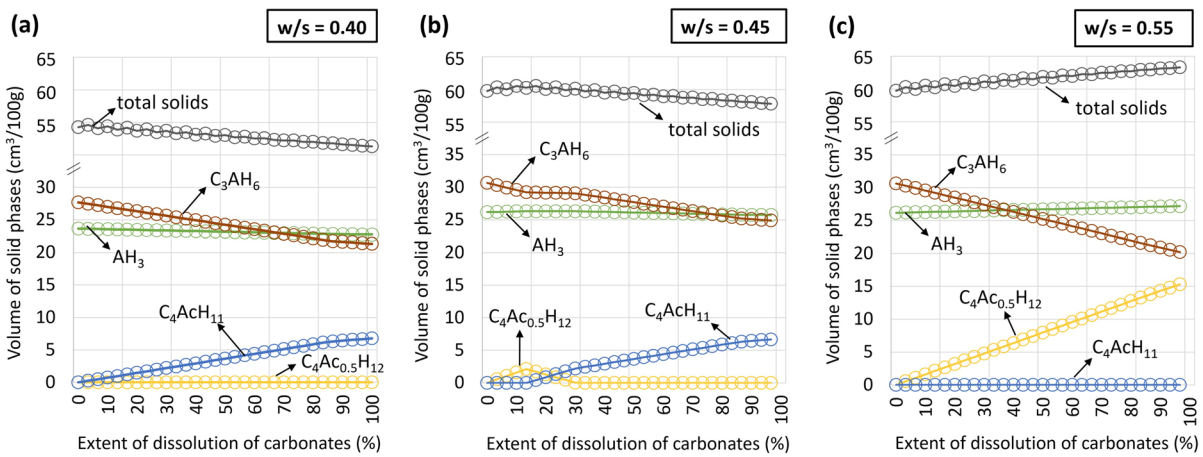

Fig. 6 Calculated phase assemblage in the CA + $CaMg(CO_3)_2$ + $FeCO_3$ system (100 g of solids) hydrated at 20 °C as a function of the degree of reaction of carbonates present in the tailings (siderite and dolomite) for: (**a**) $w/s = 0.40$, (**b**) $w/s = 0.45$, and (**c**) $w/s = 0.55$

of carbonate-containing AFm is favoured over that of C_3AH_6, even at low extents of dissolution of carbonates. This is in agreement with previous studies that propose the formation of carbonate-AFm [41–43] and even nitrate-AFm to bypass conversion in CAC [44].

A reduction in the content of carbonates in the CAC-T paste was not conclusive based on the results obtained experimentally, possibly because the content of such phases is below 1.5% of the mass of solids in the CAC-T paste and therefore within the uncertainty range of quantification in such a complex multiphase system. In addition, in all modelled scenarios, the cations released from the dissolution of carbonates are incorporated in OH-hydrotalcite (Ca^{2+}, Mg^{2+}) and ferrihydrite (Fe^{3+}). In the modelled system, such phases are predicted to form only in very minor amounts, which would be difficult to observe experimentally.

In addition to monocarbonate, the formation of small amounts (≈ 2%) of strätlingite (C_2ASH_8, indicated as Str in Fig. 4) was also observed by XRD in both CAC + Q and CAC + T pastes after 90 days. Formation of C_2ASH_8 is observed when CAC hydrates in the presence of reactive silicates, which has been proposed as a way to suppress conversion reactions [45–49]. In this study, it is suggested that C_2ASH_8 formed due to the late hydration of C_2S present in CAC (Fig. 4); therefore the suppression of conversion observed in the CAC + T paste is unlikely to result from the formation of C_2ASH_8.

Since the intermediate, metastable phases have a higher pore filling capacity i.e., the densities of C_3AH_6 (2.52 g/cm^3) and AH_3 (2.40 g/cm^3) are higher than those of CAH_{10} (1.72 g/cm^3), $C_2AH_{7.5}$ (1.98 g/cm^3), and C_2AH_8 (1.91 g/cm^3) [50], the conversion reactions induce a reduction of the volume of solids in the pastes. The effect of the conversion reactions of CAC can be observed in the pore structure of the pastes, shown in Fig. 7. Contrary to what was observed in the PC pastes, clear differences exist between the CAC + T and CAC + Q pastes, particularly at 28 days. Up to 28 days, the formation of hydration products contributed to densify the cementitious matrix and strongly overcame the adverse effect of the conversion reactions. This was observed to a lower degree in the CAC + Q paste, since the conversion reactions took place at a higher rate in that paste. Until 28 days, the remaining anhydrous CAC phases can react with the water released by the conversion

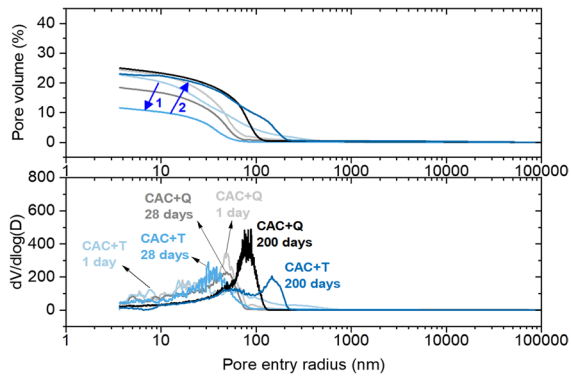

Fig. 7 Cumulative pore volume (top) and pore size distribution (bottom) of CAC pastes containing tailings (shades of blue) and reference pastes (shades of grey) hydrated for 1, 28, and 200 days. The blue arrows are a guide to the eyes and represent the order of the pore volume cumulative curves, according to the increasing age of the CAC + T paste. (Color figure online)

reactions (Eqs. 3 and 4), which will produce more pore-filling hydrates. After 28 days, however, the degree of hydration is very advanced (DoH_{28} = 88%), which limits the potential of the remaining anhydrous cement to produce significant volume of hydrates to counterbalance the conversion reactions. As a result, at prolonged hydration (200 days), the CAC + Q paste reached DoC = 90% and the pore size and total porosity increased as can be observed in the MIP results in Fig. 7. A similar effect was observed in the CAC + T paste hydrated for 200 days.

SEM–EDS analysis was carried out to investigate the microstructure of the hydrated CAC pastes. Figure 8 shows micrographs of CAC + T samples hydrated for 28 days and 200 days and CAC + Q sample hydrated for 28 days. Unreacted and partially hydrated CAC particles surrounded by a hydrated matrix can be observed, in addition to quartz and pyrite particles. The hydrated matrix contains calcium aluminate hydrates (CAH_{10}, C_2AH_x, and C_3AH_6) and AH_3 with some intermixing, as in [41]. The areas in dark grey correspond to accumulation of AH_3. In Fig. 8b, uniform lighter grey zones can be distinguished from the surrounding hydrated matrix due to a lighter grey contrast and the presence of cracks. Such cracks result from shrinkage due to loss of water during exposure to vacuum in the microscope chamber; this is typically observed in ettringite-containing systems [41]. However, the presence of ettringite

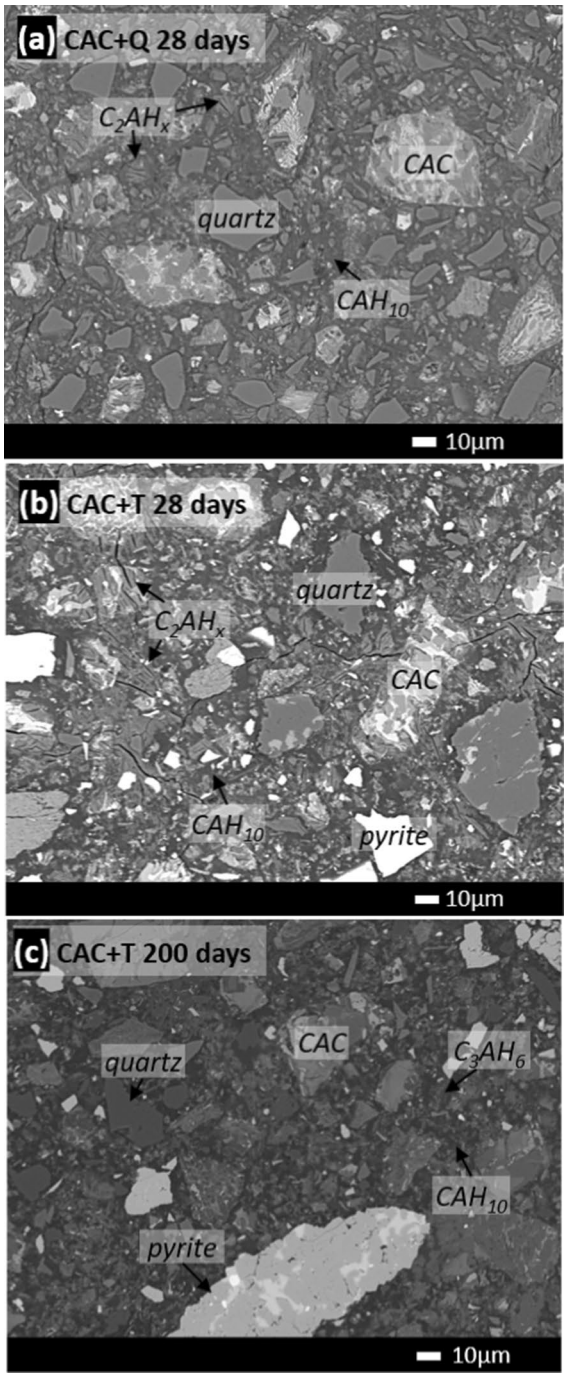

Fig. 8 SEM-BSE micrographs of (**a**) CAC + Q hydrated for 28 days, (**b**) CAC + T hydrated for 28 days, and (**c**) CAC + T hydrated for 200 days. The presence of trace minerals such as ZnS (spharelite) and a Sn, As-containing mineral within the pyrite grain is visible in (**c**). Additional micrographs and elemental maps of hydrated pastes are in Online Appendix A (Figure A-7)

in all hydrated CAC samples is not expected based on XRD results, especially in the CAC + Q paste, where sulfur sources are unavailable. The phase most likely corresponds to C_2AH_x after losing water molecules from the interlayer due to high vacuum [39]. That feature is not observed in the samples hydrated for 200 days, which is in agreement with XRD data, since those phases have converted to C_3AH_6. The large cracks observed across the hydrated matrix and CAC clinker particles were most likely caused by mechanical polishing in the preparation.

In Fig. 8b, the hydrated matrix is particularly dense, being consistent with the low total porosity verified by MIP in CAC + T pastes hydrated for 28 days. The micrograph of the CAC + T sample hydrated for 200 days (Fig. 8c) shows that the microstructure is less compact than the one observed at 28 days.

The results of the hydration studies in CAC-tailings pastes show that minor phases present in the tailings chemically interact in CAC, affecting the timing and extent of the hydrate conversion reactions typically observed in high alumina cements. Two different mechanisms act to suppress the effects of conversion: the stabilization of CAH_{10} and the formation of monocarbonate.

3.4 Hydration of calcium sulfoaluminate cement (CSA)—tailings pastes

The XRD patterns of the CSA pastes measured at different ages are shown in Fig. 9.

According to the diffraction patterns (Fig. 9), the intensity of peaks corresponding to anhydrous CSA phases (ye'elimite ($C_4A_3\bar{S}$) and anhydrite) are significantly higher in the CSA + T paste in the first 24 h, which confirm that the hydration of the CSA phases is slowed down by the tailings. In addition, the formation of hydration products—ettringite and at least two monosulfate species of different hydration states ($C_4A\bar{S}H_{14}$, indicated as M14 in Fig. 9, and $C4A\bar{S}H_{12}$, indicated as kuzelite)—is significantly less pronounced in the CSA + T paste. Such results are in good agreement with the heat flow curves, which show that by 24 h of curing the main hydration peak has passed for the reference CSA + Q paste, while in the CSA + T paste the main hydration peak has not yet occurred (Fig. 1). The calorimetry curves indicate that the differences in hydration degree level

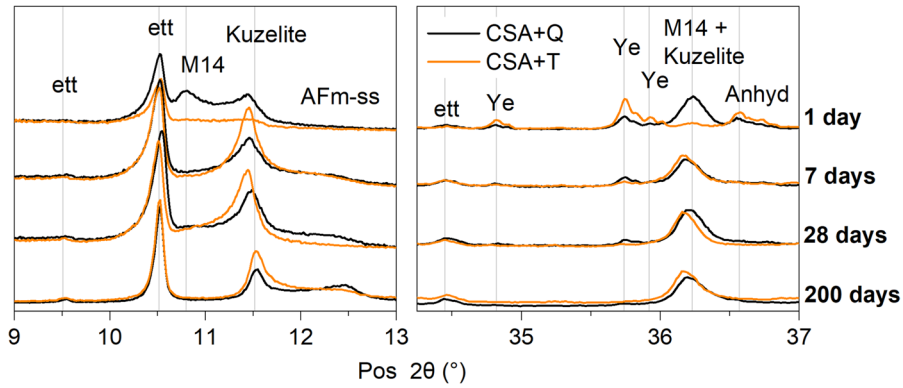

Fig. 9 XRD patterns of CSA pastes containing tailings (orange) and reference paste (black) hydrated for 1, 7, 28, and 200 days. Ett: ettringite $C_6A\overline{S}_3H_{32}$, M14: monosulfate $C_4A\overline{S}H_{14}$, Kuzelite: monosulfate $C_4A\overline{S}H_{12}$ Ye: ye'elimite $C_4A_3\overline{S}$, Anhyd: anhydrite. The XRD patterns were normalized to the intensity of the main peak of quartz ($d = 3.34$ Å). (Color figure online)

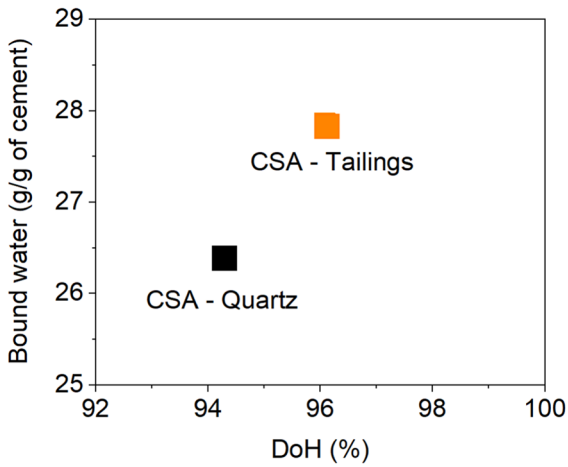

Fig. 10 Bound water content and degree of hydration (DoH) of CSA + Q and CSA + T pastes hydrated for 28 days

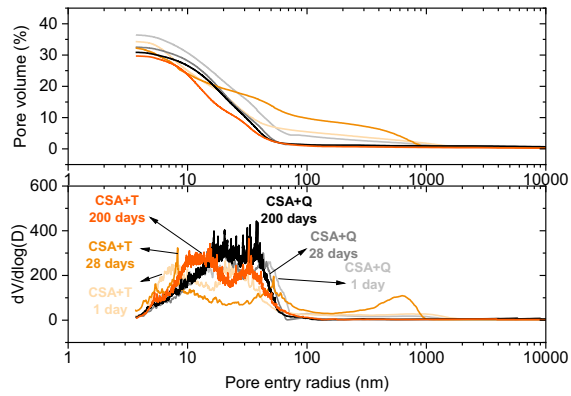

Fig. 11 Cumulative pore volume (top) and pore size distribution (bottom) of CSA pastes containing tailings (shades of orange) and reference pastes (shades of grey) hydrated for 1, 28, and 200 days. (Color figure online)

out in the following 5–6 h due to the progress of the hydration reactions in the CSA + T paste. Indeed, XRD shows that ettringite and kuzelite continuously form up to 28 days, as well as AFm solid solutions. Interestingly, higher amounts of ettringite and AFm hydrates are observed in the tailings-containing paste. This correlates with the slightly higher heat release measured up to 28 days (Fig. 1) in the CSA + T paste, as well as the higher bound water content (determined by TGA) and degree of hydration (calculated by XRD) at that age (see Fig. 10). Supporting TGA results can be found in Online Appendix A (Figure A-8).

These results show that the sulfidic tailings contribute to the hydration of the CSA paste. Given the sensitivity of CSA early hydration to the content and type of the sulfate source [51], the chemical role of the tailings is inferred to derive from the provision of additional sulfate to the CSA paste at early age. This is supported by the detection of dissolved S in the tailings leachates within the first 24 h (Online Appendix A, Figure A-5) and by the absence of the sulfate depletion peak in the heat flow curves of the CSA + T paste.

Figure 11 shows the MIP curves of the CSA pastes. In contrast with CSA + Q, which presented

a continuously refined pore structure from 1 to 200 days, the tailings-containing CSA paste was characterized by the presence of newly opened large pores at 28 days. However, after prolonged hydration (200 days), the total porosity decreased again as the large pores are no longer present.

3.5 Environmental compatibility

The environmental compatibility of the tailing-containing cements was assessed based on the results of leaching tests. Figure 12 presents the element concentrations measured in the leachates of pastes hydrated for 200 days in comparison with the threshold values for inert and non-hazardous wastes based on the European Council Directive (2003/33/EC) [52]. The reported elemental concentrations, as well as the indicated final pHs, are the averages of duplicate measurements. The concentrations of As, Co, and Zn are not presented in the Fig. 12 because they were below the detection limit for all cement pastes.

The materials tested incorporate 30 wt%. of tailings that contain significant levels of metal(loid)s, which can pose environmental and human health risks [53]. In fact, a previous study showed that a sister sample of the same material poses carcinogenic risk for adults and children due to the elevated and mobile levels of As in the tailings [53]. However, despite the moderate replacement ratio of 30 wt%, the cement pastes produced in this work present a low release of hazardous metal(loid)s (Fig. 12). The leached concentrations of all elements measured fall below the thresholds for non-hazardous waste. Moreover, except for the Pb concentrations in PC and the Sb concentrations in PC and CSA, the remaining elemental concentrations leached are below the thresholds for inert waste. These results show that the cementitious matrices of PC, CAC, and CSA were able to stabilize the contaminants present in the tailings. According to EN 12457-2, the materials produced could be classified as non-hazardous and would not pose a threat to the environment. The CSA cement matrix displayed an outstanding ability to immobilize As, Zn, Cd, Cr, Pb, Cu, and sulfates by means of incorporation into monosulfate and ettringite, as it was demonstrated in previous studies [54–56]. Further work is needed to verify if the restricted metal(loid) mobility observed here is kept in the longer term.

Given the alkaline nature of the leachates (pH > 11.4), the drainage waters generated in the landfill of crushed cement-stabilized tailings might require adequate management to enable safe discharge to surface and groundwaters. The long-term evolution of the drainage waters from the diferent cement-tailings materials depends on several factors and has not been determined. However, in drainage waters from slags and other alkaline residues, the pH can remain highly alkaline for decades [57, 58].

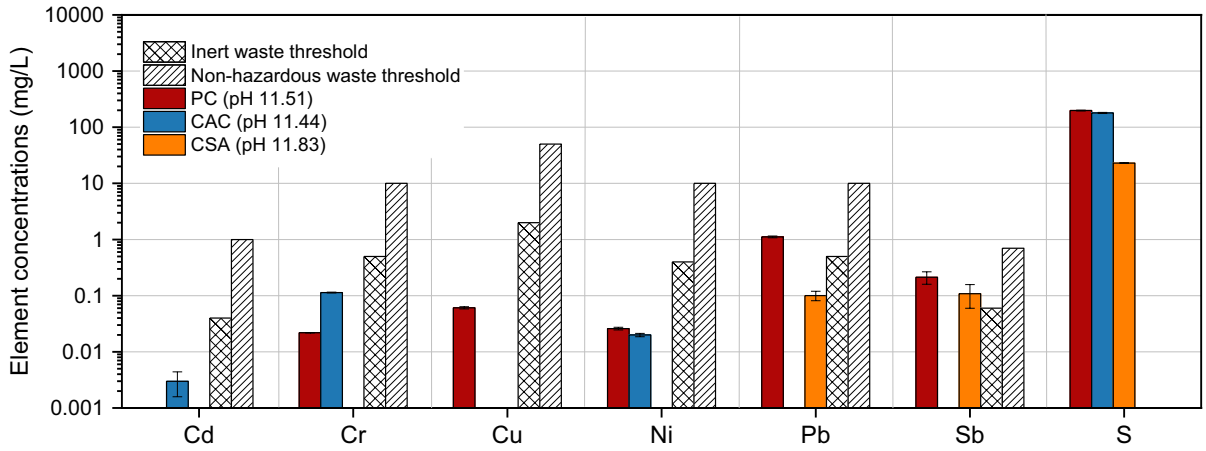

Fig. 12 Element concentrations in the leachates of cement pastes of PC, CAC, and CSA containing tailings at a 30% replacement ratio hydrated for 200 days (test EN 12457-2) compared to the threshold values for inert and non-hazardous wastes (2003/33/EC)

4 Conclusions

This experimental study demonstrated that, while in PC the tailings act as a stable admixture, they play a minor, yet active chemical role in the reduction of conversion reactions of CAC and on the formation of additional sulfate-containing hydration products in CSA. Despite the high pyrite content in the tailings, no evidence of reactions that are detrimental to the cement paste durability, such as formation of expansive phases by pyrite oxidation, was found in the hydrated pastes. The microstructure of the aged cement pastes was preserved within the studied timeframe (200 days). Moreover, all hydrated pastes containing 30 wt% tailings analyzed after 200 days of hydration presented environmental compatibility, with CSA cement being the most suitable for immobilization of metal(oid)s such as As, Zn, Cd, Cr, and Cu. Upscaling to the concrete level and long-term evaluation of concrete properties (compressive strength, volume expansion) are necessary to confirm the durability and long term stability of the sulfidic tailings in the cement-tailings systems.

Acknowledgements The authors would like to thank the European Union's Framework Programme for Research and Innovation Horizon 2020 for financial support (grant agreement #812580; SULTAN Project etn-sultan.eu). Thanks are extended to Annette Röthlisberger (IGT-ETHZ), Marion Rothaupt (IGT-ETHZ), Myrjam Mertens (SuMAT-VITO), Willem Stuyck (SuMAT-VITO), and Anne-Marie De Wilde (SuMAT-VITO) for gladly supporting the experimental work in the laboratory. Asel Maria Aguilar Sanchez (IfB-ETHZ) and Luiz Grafulha Morales (ScopeM-ETHZ) are acknowledged for their support in the preparation of samples for SEM analysis.

Author contributions NPM: Conceptualization, methodology, investigation, data analysis, visualization, writing-original draft; JH: Investigation, data analysis, writing-review and editing; MP: Investigation, writing-review and editing; RS: methodology, writing-review and editing, supervision; GH: Writing-review and editing, supervision.

Funding Open access funding provided by Swiss Federal Institute of Technology Zurich.

Declarations

Conflict of interest The authors have no relevant financial or non-financial interests to disclose.

References

1. Mudd GM, Boger DV (2013) The ever growing case for paste and thickened tailings : Towards more sustainable mine waste management. AusIMM Bull 2:56–59
2. Calvo G, Mudd G, Valero A, Valero A (2016) Decreasing Ore grades in global metallic mining: A theoretical issue or a global reality? Resources 5(4):36. https://doi.org/10.3390/resources5040036
3. Crowson P (2012) Some observations on copper yields and ore grades. Resour Policy 37(1):59–72. https://doi.org/10.1016/J.RESOURPOL.2011.12.004
4. Watari T, Nansai K, Nakajima K (2021) Major metals demand, supply, and environmental impacts to 2100: a critical review. Resour Conserv Recycl 164:105107. https://doi.org/10.1016/J.RESCONREC.2020.105107
5. Adrianto LR, Pfister S, Hellweg S (2022) Regionalized life cycle inventories of global sulfidic copper tailings. Environ Sci Technol 56(7):4553–4564. https://doi.org/10.1021/acs.est.1c01786
6. Lottermoser B (2011) Recycling, reuse and rehabilitation of mine wastes. Elements 7(6):405–410. https://doi.org/10.2113/gselements.7.6.405
7. Lottermoser B (2013) Sulfidic mine wastes. Mine Wastes. https://doi.org/10.1007/978-3-662-05133-7_2
8. Kinnunen PHM, Kaksonen AH (2019) Towards circular economy in mining: opportunities and bottlenecks for tailings valorization. J Clean Prod 228:153–160. https://doi.org/10.1016/j.jclepro.2019.04.171
9. Spooren J et al (2020) Near-zero-waste processing of low-grade, complex primary ores and secondary raw materials in Europe: technology development trends. Resour Conserv Recycl 160:104919. https://doi.org/10.1016/j.resconrec.2020.104919
10. Martins NP et al (2021) Exploring the potential for utilization of medium and highly sulfidic mine tailings in construction materials: a review. Sustainability (Switzerland) 13:12150. https://doi.org/10.3390/su132112150
11. European Committee for Standardization (CEN) (2012) EN 450-1 Fly ash for concrete—Part 1: Definition, specifications and conformity criteria
12. Associação Brasileira de Normas Técnicas (ABNT) (2014) NBR 12653: Materiais pozolânicos : requisitos
13. American Society for Testing and Materials (ASTM) (2019) ASTM C618 Standard Specification for Coal Fly

Ash and Raw or Calcined Natural Pozzolan for Use in Concrete
14. Tariq A, Nehdi M (2008) Developing durable paste backfill from sulphidic tailings. Proc Inst Civil Eng: Waste Resour Manag 160(4):155–166. https://doi.org/10.1680/warm.2007.160.4.155
15. Schmidt T, Leemann A, Gallucci E, Scrivener KL (2011) Physical and microstructural aspects of iron sulfide degradation in concrete. Cem Concr Res 41(3):263–269. https://doi.org/10.1016/j.cemconres.2010.11.011
16. Rodrigues A, Duchesne J, Fournier B, Durand B, Rivard P, Shehata M (2012) Mineralogical and chemical assessment of concrete damaged by the oxidation of sulfide-bearing aggregates: importance of thaumasite formation on reaction mechanisms. Cem Concr Res 42(10):1336–1347. https://doi.org/10.1016/j.cemconres.2012.06.008
17. Zhong R, Wille K (2018) Deterioration of residential concrete foundations: the role of pyrrhotite-bearing aggregate. Cem Concr Compos 94:53–61. https://doi.org/10.1016/j.cemconcomp.2018.08.012
18. Escobar AG, Relvas JMRS, Pinto AMM, Oliveira M (2021) Physical-chemical characterization of the neves corvo extractive mine residues: a perspective towards future mining and reprocessing of sulfidic tailings. J Sustain Metall 7(4):1483–1505. https://doi.org/10.1007/s40831-021-00428-1
19. Zunino F, Lopez M (2016) Decoupling the physical and chemical effects of supplementary cementitious materials on strength and permeability: a multi-level approach. Cem Concr Compos 65:19–28. https://doi.org/10.1016/j.cemconcomp.2015.10.003
20. Kamariah N et al (2022) Conventional versus microwave-assisted roasting of sulfidic tailings: mineralogical transformation and metal leaching behavior. Miner Eng 183:107587. https://doi.org/10.1016/J.MINENG.2022.107587
21. Zhang L, Glasser FP (2002) Hydration of calcium sulfoaluminate cement at less than 24 h. Adv Cem Res 14(4):141–155. https://doi.org/10.1680/adcr.2002.14.4.141
22. Snellings R et al (2018) RILEM TC-238 SCM recommendation on hydration stoppage by solvent exchange for the study of hydrate assemblages. Mater Struct 51(6):172. https://doi.org/10.1617/s11527-018-1298-5
23. Doebelin N, Kleeberg R (2015) Profex: a graphical user interface for the rietveld refinement program BGMN. J Appl Crystallogr 48(5):1573–1580. https://doi.org/10.1107/S1600576715014685
24. Washburn EW (1921) Note on a method of determining the distribution of pore sizes in a porous material. Proc Natl Acad Sci 7(4):115–116. https://doi.org/10.1073/pnas.7.4.115
25. Kulik DA, GEM-Selektor. PSI Villigen, Switzerland
26. Kulik DA et al (2012) GEM-Selektor geochemical modeling package: revised algorithm and GEMS3K numerical kernel for coupled simulation codes. Comput Geosci. https://doi.org/10.1007/s10596-012-9310-6
27. Wagner T, Kulik DT, Hingerl FF, Dmytrieva SV (2012) GEM-Selektor geochemical modeling package: TSolMod library and data interface for multicomponent phase models. Can Miner 50(5):1173–1195. https://doi.org/10.3749/canmin.50.5.1173
28. Lothenbach B et al (2019) Cemdata18: a chemical thermodynamic database for hydrated Portland cements and alkali-activated materials. Cem Concr Res 115:472–506. https://doi.org/10.1016/j.cemconres.2018.04.018
29. Arliguie G, Grandet J (1985) Etude par calorimetrie de l'hydratation du ciment Portland en presence de zinc. Cem Concr Res 15(5):825–832. https://doi.org/10.1016/0008-8846(85)90149-8
30. Berger S, Cau Dit Coumes C, Le Bescop P, Damidot D (2009) Hydration of calcium sulfoaluminate cement by a ZnCl2 solution: Investigation at early age. Cem Concr Res 39(12):1180–1187. https://doi.org/10.1016/j.cemconres.2009.08.003
31. Niu M, Li G, Wang Y, Li Q, Han L, Song Z (2018) Comparative study of immobilization and mechanical properties of sulfoaluminate cement and ordinary Portland cement with different heavy metals. Constr Build Mater 193:332–343. https://doi.org/10.1016/j.conbuildmat.2018.10.206
32. Wu K, Shi H, Xu L, Guo X, De Schutter G, Xu M (2014) Influence of heavy metals on the early hydration of calcium sulfoaluminate. J Therm Anal Calorim 115(2):1153–1162. https://doi.org/10.1007/s10973-013-3376-9
33. Ben Haha M, Winnefeld F, Pisch A (2019) Advances in understanding ye'elimite-rich cements. Cem Concr Res 123:105778. https://doi.org/10.1016/j.cemconres.2019.105778
34. Lothenbach B, Le Saout G, Gallucci E, Scrivener KL (2008) Influence of limestone on the hydration of Portland cements. Cem Concr Res 38(6):848–860. https://doi.org/10.1016/j.cemconres.2008.01.002
35. Lothenbach B, Pelletier-Chaignat L, Winnefeld F (2012) Stability in the system CaO–Al_2O_3–H_2O. Cem Concr Res 42(12):1621–1634. https://doi.org/10.1016/j.cemconres.2012.09.002
36. Raab B, Pöllmann H (2010) C_2AH_8–2CaO·Al_2O_3·(8±n) H2O : main hydration products of CAC. In : European powder diffraction conference; Darmstadt, Germany, Oldenbourg Wissenschaftsverlag, pp 349–354. https://doi.org/10.1524/9783486991321-058
37. Ideker JH, Scrivener KL, Fryda H, Touzo B (2019) Calcium aluminate cements. https://doi.org/10.1016/B978-0-08-100773-0.00012-5
38. Midgley HG, Midgley A (1975) The conversion of high alumina cement. Mag Concr Res 27(91):43–53. https://doi.org/10.1680/macr.1975.27.91.59
39. Ukrainczyk N, Matusinovic T, Kurajica S, Zimmermann B, Sipusic J (2007) Dehydration of a layered double hydroxide-C2AH8. Thermochim Acta 464(1–2):7–15. https://doi.org/10.1016/j.tca.2007.07.022
40. Dosch W, Koestel C (1978) Stabilized dicalcium aluminate hydrates. US4095989A
41. Bizzozero J, Scrivener KL (2015) Limestone reaction in calcium aluminate cement-calcium sulfate systems. Cem Concr Res 76:159–169. https://doi.org/10.1016/j.cemconres.2015.05.019

42. Kuzel HJ, Baier H (1996) Hydration of calcium aluminate cements in the presence of calcium carbonate. Eur J Miner 8(1):129–142. https://doi.org/10.1127/ejm/8/1/0129
43. Luz AP, Pandolfelli VC (2012) $CaCO_3$ addition effect on the hydration and mechanical strength evolution of calcium aluminate cement for endodontic applications. Ceram Int 38(2):1417–1425. https://doi.org/10.1016/J.CERAMINT.2011.09.021
44. Falzone G, Balonis M, Sant G (2015) X-AFm stabilization as a mechanism of bypassing conversion phenomena in calcium aluminate cements. Cem Concr Res 72:54–68. https://doi.org/10.1016/j.cemconres.2015.02.022
45. Heikal M, Morsy MS, Radwan MM (2005) Electrical conductivity and phase composition of calcium aluminate cement containing air-cooled and water-cooled slag at 20, 40 and 60 °C. Cem Concr Res 35(7):1438–1446. https://doi.org/10.1016/J.CEMCONRES.2004.09.027
46. Astoveza J, Trauchessec R, Soth R, Pontikes Y (2021) Properties of calcium aluminate blended cement incorporating iron-rich slag: evolution over a curing period of 1 year. Constr Build Mater 282:122569. https://doi.org/10.1016/J.CONBUILDMAT.2021.122569
47. Ding J, Fu Y, Beaudoin JJ (1995) Strätlingite formation in high alumina cement: silica fume systems—significance of sodium ions. Cem Concr Res 25(6):1311–1319. https://doi.org/10.1016/0008-8846(95)00124-U
48. Majumdar AJ, Singh B (1992) Properties of some blended high-alumina cements. Cem Concr Res 22(6):1101–1114. https://doi.org/10.1016/0008-8846(92)90040-3
49. Edmonds RN, Majumdar AJ (1989) The hydration of mixtures of monocalcium aluminate and blastfurnace slag. Cem Concr Res 19(5):779–782. https://doi.org/10.1016/0008-8846(89)90048-3
50. Roberts MH (2007) New calcium aluminate hydrates. J Appl Chem 7(10):543–546. https://doi.org/10.1002/jctb.5010071004
51. Winnefeld F, Barlag S (2010) Calorimetric and thermogravimetric study on the influence of calcium sulfate on the hydration of ye'elimite. J Therm Anal Calorim 101(3):949–957. https://doi.org/10.1007/s10973-009-0582-6
52. Directive 2003/33/EC (2003) Directive 2003/33/EC of the European Parliament and of the Council of 26 May 2003 on the approximation of the laws, regulations and administrative provisions of the Member States relating to the advertising and sponsorship of tobacco products. https://eur-lex.europa.eu/legal-content/EN/TXT/HTML/?uri=CELEX:32003L0033
53. Helser J, Vassilieva E, Cappuyns V (2022) Environmental and human health risk assessment of sulfidic mine waste: bioaccessibility, leaching and mineralogy. J Hazard Mater 424:127313. https://doi.org/10.1016/j.jhazmat.2021.127313
54. Kiventerä J, Piekkari K, Isteri V, Ohenoja K, Tanskanen P, Illikainen M (2019) Solidification/stabilization of gold mine tailings using calcium sulfoaluminate-belite cement. J Clean Prod 239:118008. https://doi.org/10.1016/j.jclepro.2019.118008
55. Piekkari K, Ohenoja K, Isteri V, Tanskanen P, Illikainen M (2020) Immobilization of heavy metals, selenate, and sulfate from a hazardous industrial side stream by using calcium sulfoaluminate-belite cement. J Clean Prod 258:120560. https://doi.org/10.1016/j.jclepro.2020.120560
56. Peysson S, Péra J, Chabannet M (2005) Immobilization of heavy metals by calcium sulfoaluminate cement. Cem Concr Res 35(12):2261–2270. https://doi.org/10.1016/j.cemconres.2005.03.015
57. Riley AL, Mayes WM (2015) Long-term evolution of highly alkaline steel slag drainage waters. Environ Monit Assess 187(7):463. https://doi.org/10.1007/s10661-015-4693-1
58. Gomes HI, Mayes WM, Rogerson M, Stewart I, Burked IT (2016) Alkaline residues and the environment: a review of impacts, management practices and opportunities. J Clean Prod 112:3571–3582. https://doi.org/10.1016/J.JCLEPRO.2015.09.111